

Direct synthesis of hydrogen peroxide on zirconia-supported catalysts under mild conditions

Stefano Melada, Riccardo Rioda, Federica Menegazzo, Francesco Pinna, Giorgio Strukul *

Dipartimento di Chimica, Università di Venezia, and Consorzio INSTM, Dorsoduro 2137, 30123 Venezia, Italy

Received 20 February 2006; revised 21 February 2006; accepted 23 February 2006

Available online 23 March 2006

Abstract

Palladium catalysts supported on SO_4^{2-} -, Cl^- -, F^- -, and Br^- -doped zirconia were tested for the direct synthesis of hydrogen peroxide under very mild (1 bar and 20 °C) and nonexplosive conditions. The catalysts were characterized by thermogravimetric/differential scanning calorimetry analysis, N_2 physisorption, and temperature-programmed reduction before and after catalytic tests to investigate the oxidation state of the metal. The catalytic tests were carried out in different solvents, and the effect of the Pd oxidation state was ascertained. The best catalytic results were observed in methanol, using H_2/O_2 mixtures containing a large excess of oxygen and using the sulfate-doped zirconia catalyst. Surface-oxidized Pd^0 catalysts showed high catalytic activity and the highest selectivity.

© 2006 Elsevier Inc. All rights reserved.

Keywords: Hydrogen peroxide direct synthesis; Palladium; Zirconia; Sulfate

1. Introduction

The direct synthesis of H_2O_2 has been known since the beginning of the 20th century [1] but has not yet found industrial application because of severe drawbacks related mainly to the hazardous nature of H_2/O_2 gas mixtures and the low H_2O_2 yield that can be reached with known catalysts based on palladium. But the increasing demand for hydrogen peroxide [2] from several industrial sectors, including the pulp and paper industry and wastewater treatment, as well as the general need for greener oxidants has rekindled interest in finding an alternative to the anthraquinone route [3], which currently is almost the only process used worldwide, with a >90% share. This process, based on the anthraquinone/anthrahydroquinone redox pair, has the advantage of avoiding direct mixtures of H_2 and O_2 . Nevertheless, it produces significant amounts of organic waste due to the overreduction of anthraquinone, it requires several separation and concentration steps, and it is economically feasible only in large-scale plants.

Several patents concerning the direct synthesis of H_2O_2 [4–8] and a number of scientific papers [9–16] have appeared over the last decades, with Pospelova and coworkers pioneering the field in the 1960s [9,17]. Most of these patents and papers deal with explosive hydrogen/oxygen mixtures and very high pressures, which are necessary to improve H_2O_2 selectivity. The first industrial attempt to prepare H_2O_2 via direct synthesis was carried out in the 1980s by Du Pont [4,5,18,19]. For the first time, the use of such additives as halogenides (especially bromide [5]) and organophosphates [19] was suggested to improve the selectivity of carbon-supported Pd [4] and Pd/Pt catalysts [18]. The synthesis was carried out under high pressure (up to 170 bar), but this process was never scaled-up, because of serious explosion risks.

Direct synthesis using various technologies, including modified fuel cells [20–22], new water electrolysis processes able to simultaneously produce hydrogen and hydrogen peroxide [23,24], and nonequilibrium plasma systems [25], has been proposed. These technologies, although fascinating, consume very high amounts of energy and demonstrate—at least at the moment—low overall efficiency. Some patents [26,27] and scientific papers [28,29] have also addressed the use of catalytic membranes to avoid direct contact between H_2 and O_2 in the

* Corresponding author. Fax: +39 041 234 8517.
E-mail address: strukul@unive.it (G. Strukul).

gas phase. The use of membranes is very promising, but far from industrially applicable.

This work reports the preparation and use of Pd-supported catalysts for the direct synthesis of hydrogen peroxide that can be carried out under very mild conditions. Zirconia was chosen as the support, because it has desirable properties, including tuneable surface acidity/basicity (controlled by the addition of different dopants), redox properties, and tuneable porosity and surface area. In particular, sulfating zirconia [30] not only causes modification of the acid properties, but also affects surface features; sulfates retard crystallization, stabilize the tetragonal phase, and improve surface area and pore size. Because H_2O_2 is more stable under acidic conditions, a strongly acidic support (doped with SO_4^{2-} , Cl^- , F^- , or Br^-) may be useful for the direct synthesis of H_2O_2 .

2. Experimental

2.1. Materials

ZrOCl_2 (Fluka), $(\text{NH}_4)_2\text{SO}_4$ (Merck), NH_4F (Fluka), NH_4Br (Fluka), and NH_4Cl (Carlo Erba) were used as received for sample synthesis. All kinetic tests were performed in anhydrous methanol (SeccoSolv, Merck, $[\text{H}_2\text{O}] < 0.005\%$) and ethanol (SeccoSolv, Merck, $[\text{H}_2\text{O}] < 0.02\%$). Commercial standard solutions of $\text{Na}_2\text{S}_2\text{O}_3$ (Fixanal [0.01], Hydranal-solvent E, and Hydranal-titrant 2E, all from Riedel-de Haen) were used for iodometric and Karl–Fischer titrations.

2.2. Methods

Surface areas and pore size distributions were obtained from N_2 adsorption/desorption isotherms at -196°C (using a Micromeritics ASAP 2000 analyser). Calcined samples were pretreated at 300°C for 2 h under vacuum. The noncalcined sample was pretreated at 150°C for 4 h under vacuum. Surface area was calculated from the N_2 adsorption isotherm by the BET equation, and pore size distribution was determined by the BJH method also applied on the adsorption branch [31]. Total pore volume was taken at $p/p_0 = 0.99$.

Thermogravimetric/differential scanning calorimetry (TG/DSC) analyses were performed on a NETZSCH STA 409C instrument in flowing air (40 ml/min) at a temperature rate of $10^\circ\text{C}/\text{min}$ in the 25 – 1000°C range. Temperature-programmed reduction (TPR) experiments were carried out in a homemade apparatus. Samples (100 mg) were heated at a rate of $10^\circ\text{C}/\text{min}$ from 25 to 450°C in a 5% H_2/Ar reducing mixture (40 ml/min STP). Actual metal loading was determined by atomic absorption spectroscopy after microwave disaggregation of the samples (50 mg).

2.3. Catalyst preparation

Zirconia support was prepared by precipitation from ZrOCl_2 at constant pH (pH = 10), aged under reflux conditions [32,33], washed free from chloride (AgNO_3 test), and dried at 110°C

overnight. This material was impregnated by an incipient wetness method with various anions, using $(\text{NH}_4)_2\text{SO}_4$, NH_4F , NH_4Br , and NH_4Cl in amounts necessary to yield an 8 wt% anion loading. Impregnated supports were then calcined in flowing air (50 ml/min) at 500°C (sulfate-doped zirconia at 650°C) for 3 h. Calcined supports were subsequently impregnated by incipient wetness with a H_2PdCl_4 solution to give a nominal 2.5 wt% Pd-loaded catalyst and finally calcined again at 500°C in flowing air for 3 h.

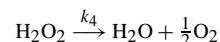
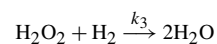
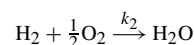
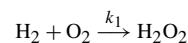
2.4. H_2O_2 synthesis

Catalytic tests were carried out at atmospheric pressure in a 20°C thermostatted glass reactor. Mixing was carried out with a Teflon rotor operating at 1000 rpm. Air, hydrogen, and nitrogen were bubbled by a gas diffuser directly into the liquid phase, at a total flow of 50 ml/min. The final gas mixture had the following composition: $\text{H}_2:\text{O}_2:\text{N}_2 = 10:10:80$. (Caution: this is just outside the explosion range, but not outside the flammable range.) Catalysts were introduced wet rather than in the dry state. In addition, because a ring of Pd catalyst tends to form above the reaction mixture during catalytic experiments, the reactor slurry was swirled so as to remove the solid from the reactor wall. For some experiments, a nonexplosive, nonflammable $\text{H}_2:\text{O}_2$ 4:96 mixture was used instead of the air–hydrogen–nitrogen mixture. The reaction medium was 100 ml of a 0.03 M H_2SO_4 aqueous, ethanolic, or methanolic solution and was presaturated with the gas mixture before introduction of the catalyst (135 mg). If not otherwise indicated, catalysts were neither reduced nor pretreated before use.

During the catalytic tests, small aliquots of the liquid phase were sampled through a septum and used for water and hydrogen peroxide determination. H_2O_2 concentration was measured by iodometric titration, and water was determined by the volumetric Karl–Fischer method. H_2O_2 selectivity at time t was determined as follows:

$$S_{\text{H}_2\text{O}_2} = \frac{[\text{H}_2\text{O}_2]}{[\text{H}_2\text{O}_2] + [\text{H}_2\text{O}]}$$

A simple model was used to fit the kinetic data and find the apparent kinetic constants of the four reactions involved in the catalytic process (see Scheme 1). We accounted only for H_2O_2 decomposition by H_2 reduction and did not consider the H_2O_2 disproportionation reaction, because the latter is negligible under our reaction conditions [47].



Scheme 1.

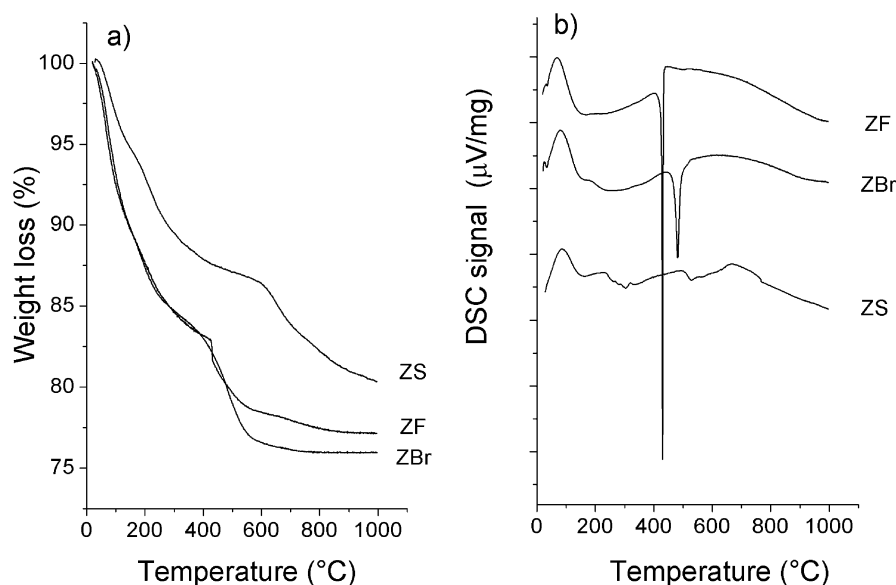


Fig. 1. TG (a) and DSC (b) profiles of doped zirconia supports.

$$\frac{dc_{\text{H}_2}}{dt} = -k_1 c_{\text{H}_2}^a c_{\text{O}_2}^b - k_2 c_{\text{H}_2}^c c_{\text{O}_2}^d - k_3 c_{\text{H}_2\text{O}_2}^e c_{\text{H}_2}^e$$

$$\frac{dc_{\text{O}_2}}{dt} = -k_1 c_{\text{H}_2}^a c_{\text{O}_2}^b - k_2 c_{\text{H}_2}^c c_{\text{O}_2}^d$$

$$\frac{dc_{\text{H}_2\text{O}_2}}{dt} = k_1 c_{\text{H}_2}^a c_{\text{O}_2}^b - k_3 c_{\text{H}_2\text{O}_2}^e c_{\text{H}_2}^e$$

$$\frac{dc_{\text{H}_2\text{O}}}{dt} = k_2 c_{\text{H}_2}^c c_{\text{O}_2}^d + 2k_3 c_{\text{H}_2\text{O}_2}^e c_{\text{H}_2}^e$$

Scheme 2.

In the system of differential equations coming from mass balance (see Scheme 2), the concentrations of H_2 and O_2 into the liquid phase can be considered constant, because these reagents are fed continuously into the semibatch reactor. Their concentrations can be incorporated into the kinetic constants, k_n , to give apparent kinetic constants, k'_n , and the resulting system of differential equations can be solved for the H_2O_2 and H_2O concentrations to give

$$c_{\text{H}_2\text{O}_2} - c_{\text{H}_2\text{O}_2}^0 = \frac{k'_1}{k'_3} (1 - e^{-k'_3 t})$$

and

$$c_{\text{H}_2\text{O}} - c_{\text{H}_2\text{O}}^0 = (k'_2 + 2k'_1 + 2k'_3 c_{\text{H}_2\text{O}_2}^0) t - 2 \frac{k'_1}{k'_3} (1 - e^{-k'_3 t}).$$

Catalytic tests data fitting was carried out with a computer program OriginLab OriginPro7.5, equipped with a special fitting tool (based on the Levenberg–Marquardt algorithm) to perform nonlinear regression analysis.

3. Results and discussion

3.1. TG/DSC analyses

Initial TG/DSC analyses were carried out on uncalcined supports to observe the material behavior during calcination. Fig. 1 reports the TGA and DSC profiles for SO_4^{2-} , Br^- , and F^- -doped uncalcined samples. As can be seen (Fig. 1a), all samples showed significant weight loss from room temperature to about 300 °C due to water desorption and surface dehydroxylation processes. At about 480–500 °C, ZF and ZBr showed further weight loss, which can be reasonably attributed to doping salt decomposition. This process shifted to higher temperatures (600–650 °C) for the ZS sample. Above 600 °C, the ZF and ZBr profiles showed no significant weight loss, whereas the ZS support showed weight loss up to 1000 °C. In the DSC profiles (Fig. 1b), the endothermic nature of water desorption (around 100 °C) and dehydroxylation (around 250 °C) processes can be observed. The DSC profile of ZF sample showed a sharp exothermic peak at 480 °C due to ammonium salt decomposition, which can be associated with the weight loss already observed on the TG analysis. Similarly, the DSC spectrum of ZBr support exhibited an analogous exothermic peak at slightly higher temperature (520 °C). Zirconia-phase transition and doping salt decomposition for ZF and ZBr samples occurred at approximately the same temperature and were associated with the exothermic peaks at 480–520 °C. The ZS profile showed two distinct peaks [34–36]: an exothermic one occurring without weight loss, which can be associated with zirconia-phase transition (from amorphous to crystalline), and a second endothermic peak at higher temperatures, associated with weight loss, related to sulfate decomposition.

To prove this point, an undoped zirconia sample (Z) was also prepared, but this is not reported in Fig. 1 for the sake of simplicity. In agreement with the literature [37], this sample showed the same weight loss of doped samples up to 400 °C, as-

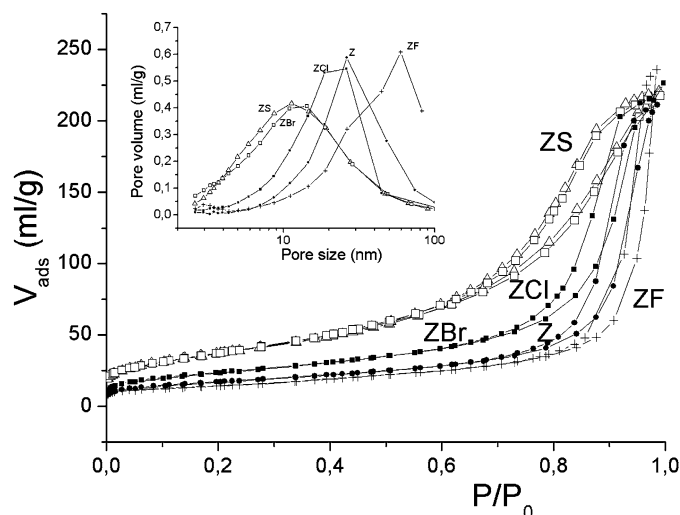


Fig. 2. N_2 physisorption isotherms of calcined samples and (insert) BJH pore size distributions of calcined samples: (Δ) ZS, (\square) ZBr, (\blacksquare) ZCl, (+) ZF, (\bullet) Z.

Table 1
Surface features of calcined samples and Pd loading on final catalysts

Sample	SSA (m^2/g)	Pore diameter (nm)	Pore volume (cm^3/g)	Pd loading (wt%)
ZS	134	10.2	0.341	2.64
ZF	50	29.0	0.364	2.45
ZBr	135	9.9	0.336	2.65
ZCl	85	16.4	0.349	2.82
Z	61	21.3	0.327	2.91

sociated with water desorption and dehydroxylation. At higher temperatures, no further weight loss was observed. Only a sharp exothermic peak at about $460^\circ C$ was recorded, associated with crystallization of the amorphous oxide.

3.2. N_2 physisorption analyses

The N_2 physisorption isotherms for the calcined samples are reported in Fig. 2. As can be seen, all samples showed type IV isotherms with hysteresis loops typical of mesoporous materials. A noncalcined, nondoped zirconia precursor (not shown) was mesoporous (BJH mean pore size 5.5 nm) but showed a high fraction of microporosity and a high surface area ($424 m^2/g$). This fragile amorphous structure almost collapsed after calcination to produce a mesoporous to macroporous material, with surface area of $50\text{--}80 m^2/g$. All N_2 physisorption data are reported in Table 1, along with Pd loadings determined on the final catalysts. Treatment with fluoride anions produced samples very similar to the nondoped sample; fluoride did not prevent structure collapse and pore wall thickening. The resulting materials had low surface areas ($50\text{--}60 m^2/g$) and a macroporous structure (pore size >20 nm). Sulfate and bromide doping yielded materials retaining high surface area ($130\text{--}140 m^2/g$) and a mesoporous structure (mean pore size around 10 nm). These ions strongly bind the material, avoiding, or at least retarding, structure collapse. Chloride ions had an

intermediate effect; surface area was $85 m^2/g$, and mean pore size was around 15 nm.

3.3. TPR analysis of fresh catalysts

After Pd deposition and calcination, TPR analysis was performed to investigate the metal oxidation state. The TPR testing setup requires that the reducing mixture pass through the samples to be analysed before starting the temperature ramp, to clean the apparatus. This procedure can cause PdO reduction already at room temperature. In fact PdO obtained after calcination can be reduced already at $-15^\circ C$, and if the Pd metal particles are large enough, they can lead to the formation of Pd β -hydride [38,39]. It is well known that Pd β -hydride decomposes at about $70^\circ C$. Therefore, the calcined samples that contain reducible PdO should show a negative peak at about $70^\circ C$ due to Pd β -hydride decomposition. Fig. 3a shows the TPR profiles for all freshly calcined samples. In agreement with the above, ZF-PdO and ZS-PdO samples showed a negative Pd β -hydride decomposition peak at about $70^\circ C$. The other samples did not show room temperature-reducible Pd(II) species; they all possessed only PdO reducible at about $90\text{--}100^\circ C$. This species is present also in ZF-PdO and ZS-PdO, along with another Pd(II) fraction that reduced at about $280\text{--}300^\circ C$. This may be residual palladium(II) oxychloride, formed during calcination and not decomposed during thermal treatment.

The brownish color of all of the samples after calcination indicated that Pd was oxidized. After TPR analysis, all samples were completely black. Notably, the high temperature region of ZS-PdO TPR profile showed massive hydrogen consumption, which can reasonably be attributed to sulfate reduction to SO_2 and H_2S [33].

3.4. Catalytic data

All catalytic tests were carried out under very mild conditions (1 bar and $20^\circ C$) and with dilute H_2/O_2 mixtures, well away from the explosive regime. Preliminary tests of H_2O_2 decomposition were carried out on pure calcined supports under the same experimental conditions, to verify that they did not decompose H_2O_2 over the 2-h test. In fact, as reported in Scheme 1, numerous reactions are involved in the direct synthesis of hydrogen peroxide (all catalyzed by Pd), and the major problem of this process is the low selectivity.

The effect of different solvents was studied. The samples were first tested in aqueous solution; the results are reported in Fig. 4. As reported previously [29], in this solvent, estimating the amount of produced water, and hence the selectivity, is impossible. During these tests, all catalysts turned from dark brown to black in less than 15 min, with only minor differences in activity observed among the samples. H_2O_2 concentrations of $3.2\text{--}4.4$ mM were produced within 2 h. Catalyst productivities, expressed as $mmol_{H_2O_2}/(g_{Pd}h)$, ranged from 42 for ZCl-PdO to 66 for ZF-PdO after 120 min time on stream. Reactivity tests in water showed that our samples have relatively good catalytic activity toward H_2O_2 direct synthesis. Nevertheless, the production of H_2O_2 in solvents other than water is

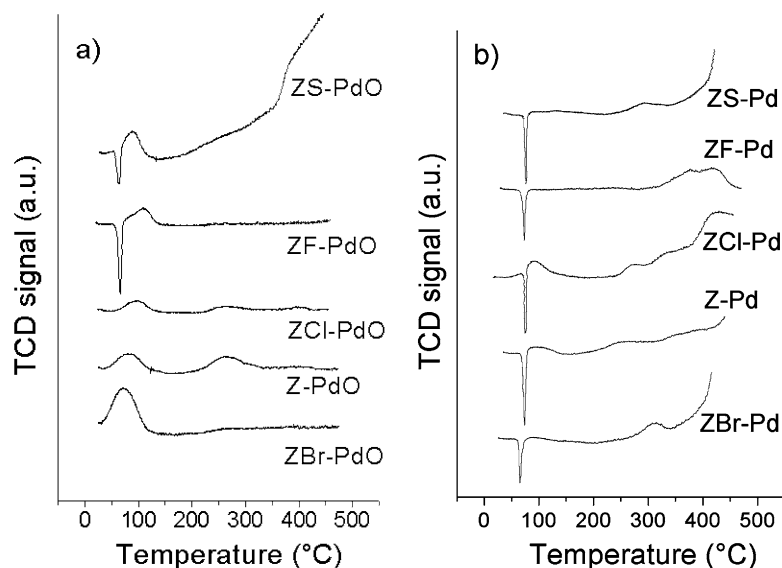


Fig. 3. TPR profiles of fresh calcined catalysts (a) and exhausted catalysts (b).

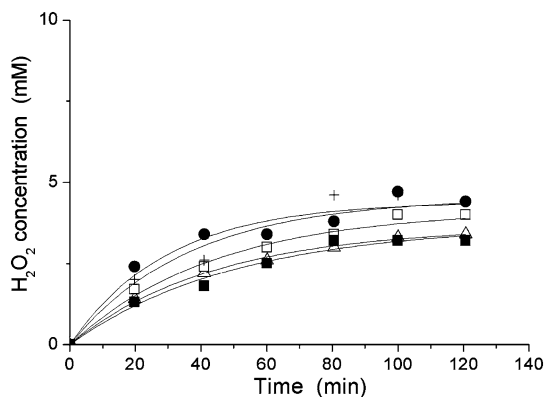


Fig. 4. Catalytic activity during kinetics tests in aqueous solutions: (Δ) ZS-PdO, (\square) ZBr-PdO, (\blacksquare) ZCl-PdO, (+) ZF-PdO, (\bullet) Z-PdO.

desirable for several reasons: (i) most oxidation reactions involving H₂O₂ are carried out in organic solvents, like alcohols; (ii) hydrogen and oxygen solubilities in organic compounds are usually higher than those in water; (iii) dry organic media allow measurement of the water produced, thus giving an estimate of catalyst selectivity. For these reasons, the next tests were carried out in alcohols, such as ethanol and methanol, which several patents [4,40,41] and scientific papers [10,13] have reported to be excellent solvents for H₂O₂ synthesis. Recently, for example, Lunsford et al. reported that ethanol is superior to water as the medium for direct formation of H₂O₂ from H₂ and O₂ over a palladium catalyst [42]. Under our experimental conditions, we found a similar trend, as shown in Fig. 5a for ethanol solutions. It can be observed that productivity is, as expected, higher than in water, ranging from 59 to 155 mmolH₂O₂/(gPd h) after 120 min of time on stream. The nonpromoted Z-PdO sample showed the lowest H₂O₂ production; ZS-PdO demonstrated the maximum H₂O₂ concentration, about 12 mM. The other samples behaved similarly but with lower productivity, yielding about 9 mM within 2 h. The profiles of H₂O formation shown in Fig. 5a allow calculation of selectivity trends as well

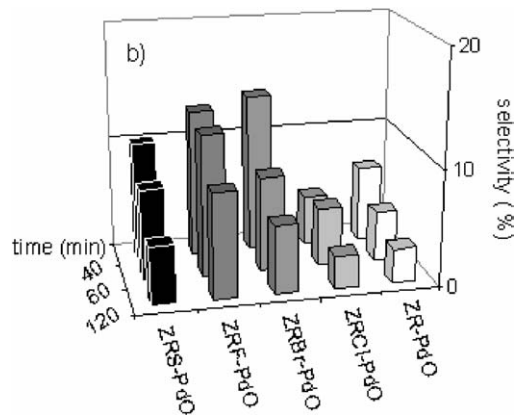
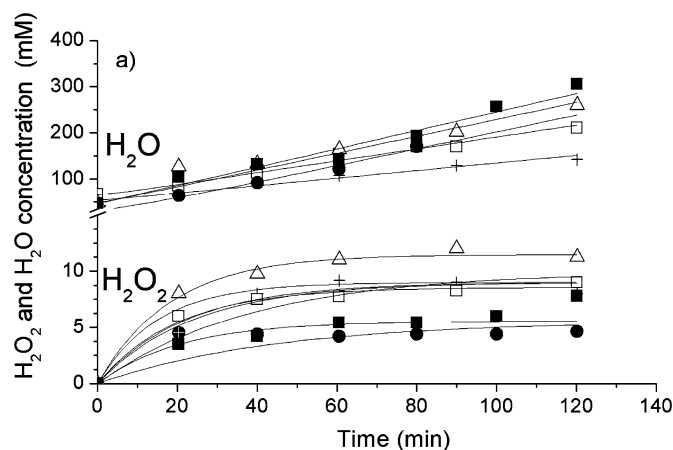


Fig. 5. Catalytic activity (a) and selectivity (b) towards H₂O₂ during kinetics tests in ethanol: (Δ) ZS-PdO, (\square) ZBr-PdO, (\blacksquare) ZCl-PdO, (+) ZF-PdO, (\bullet) Z-PdO.

(Fig. 5b). The best initial selectivity was shown by the bromide- and fluoride-promoted samples, with the latter preserving 9% selectivity after 2 h. The nondoped and Cl⁻ doped samples showed the worst selectivity trends. During tests in ethanol, all samples changed color from dark brown to black within a few

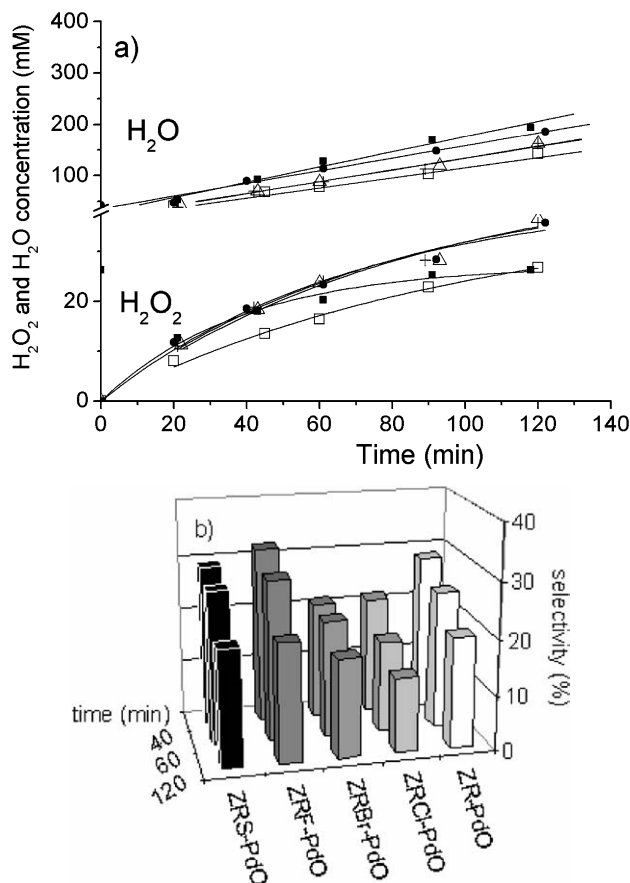


Fig. 6. Catalytic activity (a) and selectivity (b) towards H₂O₂ during kinetics tests in methanol: (△) ZS–PdO, (□) ZBr–PdO, (■) ZCl–PdO, (+) ZF–PdO, (●) Z–PdO.

minutes. It is interesting to note that ZS–PdO and, to a lesser extent, ZF–PdO, showed a decreasing H₂O₂ concentration curve after 100 min. This means that beyond that point, H₂O₂ decomposition begins to prevail over H₂O₂ formation.

All calcined samples were also tested in methanol; the results are reported in Fig. 6. The following observations can be drawn from Fig. 6a: (i) ZS–PdO, ZF–PdO, and nondoped ZPdO have about the same productivity and selectivity, showing the best catalytic results; (ii) the maximum H₂O₂ concentration obtained was about 36 mM, which corresponds to a productivity of 520 mmol_{H₂O₂}/(g_{Pd} h); (iii) ZCl–PdO was quite active at the beginning, but after 1 h time on stream, its productivity dropped significantly (with the H₂O₂ decomposition rate predominating); and (iv) ZBr–PdO showed the worst performance. Fig. 6b reports the selectivities for these reactions. The SO₄²⁻- and F⁻-promoted and nonpromoted samples behaved very similarly. The highest initial selectivity (32%) was observed for the ZF–PdO sample; ZS–PdO and Z–PdO started from about the same value (29%). The final selectivity for these samples was about the same, ranging around 20–21%. ZCl–PdO, despite its high initial productivity, showed low selectivity (from 21 to 13%) over the test duration. ZBr–PdO selectivity ranged from an initial value of 21% to a final value of 18%.

Table 2

Kinetic constants of tests in methanol using the hydrogen/air/nitrogen gas mixture

Sample	$k'_1 \times 10^4$ (mol/(l min))	$k'_2 \times 10^4$ (mol/(l min))	$k'_3 \times 10^2$ (min ⁻¹)
ZS–PdO	5.3	8.7	1.1
ZF–PdO	5.6	7.8	1.3
ZBr–PdO	3.7	8.9	1.0
ZCl–PdO	7.0	10.8	2.6
Z–PdO	5.5	9.4	1.2

3.5. Kinetic analysis

Fitting the catalytic curves shown in Fig. 6 according to the procedure specified in the Experimental section yielded the parameters reported in Table 2. Note that ZCl–PdO had the highest k' values. This means that it was the most active sample, but its activity toward H₂O producing reactions (k'_2 and k'_3) was higher than that toward H₂O₂ synthesis (k'_1). ZBr–PdO, as expected, showed the lowest k' values. Finally, ZS–PdO, ZF–PdO, and ZPdO had similar k' values. The k'_3 decomposition constants were about the same for the SO₄²⁻-, F⁻-, and Br⁻-doped samples and the nondoped samples, meaning that all of these samples behaved similarly toward H₂O₂ decomposition, in agreement with the observation of Lunsford et al. [43] that decomposition rate is affected mainly by acidity and to a lesser extent by the doping anion. Instead, ZCl–PdO had a k'_3 more than double that of the other samples, accounting for the high decomposition rate and a high H₂O formation observed with this catalyst.

Bromide ion was claimed to block very active water-producing sites [5,18,44,45], thereby improving the selectivity toward H₂O₂. However, excess bromide was detrimental to catalytic activity [46,47]. In the present case, the starting 8% bromide deposited on zirconia was probably high, because during activity tests some bromide ions might be leached into solution and reabsorbed on the Pd particle surface, extensively poisoning it.

3.6. Used samples

TPR analysis of the used samples, shown in Fig. 3b, can provide insight into some of the catalytic results reported above. First, it is evident that Pd in all samples is completely reduced during catalytic tests. This is demonstrated by the presence of the Pd β-hydride decomposition peak and the absence of any reduction peak in the same region. Only the ZCl–PdO TPR profile showed a significant amount of Pd(II) species, still nonreducible under the experimental conditions used. Interestingly, most samples showed a reduction peak above 350 °C, which can be associated with sulfate decomposition. This can explain the similar behavior of ZS–PdO and, quite unexpectedly, Z–PdO. Sulfate ions, coming from sulphuric acid added to acidify the solution in catalytic tests, can adsorb on the unpromoted zirconia surface, changing it to an actual sulfated zirconia sample. In fact, it has been reported previously [45,48,49] that unpromoted zirconia samples have a great ability to de-

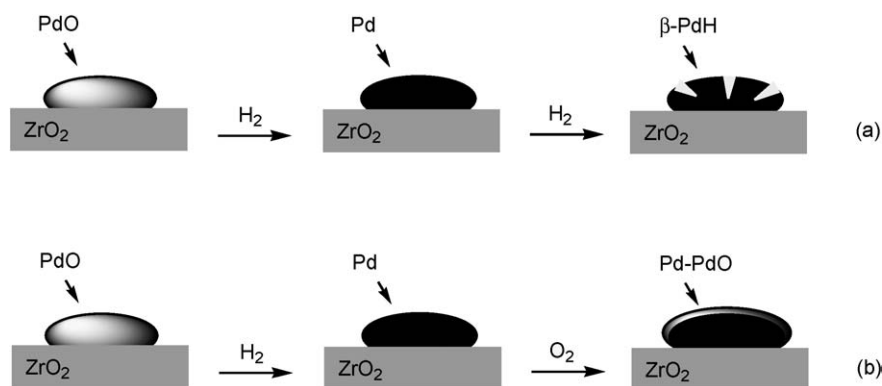


Fig. 7. Pd particle reduction during catalytic tests: possible structural changes during catalytic tests (a), Pd particle changes during catalyst pre-treatment (b).

compose H₂O₂. Sulfate adsorption on the surface, as in our case, could block those coordinatively unsaturated Zr⁴⁺ sites able to decompose H₂O₂ molecules. Moreover, the ZCl–PdO and ZBr–PdO samples adsorbed significant amounts of sulfate, which could indicate that halogenides were possibly released in solution while sulfate ions were adsorbed onto the zirconia surface. Therefore, bromide ion could adsorb onto the Pd particle surface, poisoning it. Because the amount of Br[−] carried by the catalyst was quite high (8 wt%), the extent of active site poisoning likely was beyond the beneficial amount. Chloride ions can dissolve in methanol and re-adsorb onto the Pd surface, but in this case the effect is more complicated. Choudhary [45] reported, in agreement with our data, that chlorination increased the H₂O₂ decomposition rate by about one order of magnitude with respect to that of brominated Pd/zirconia catalyst. However, in the same paper, Choudhary also reported that fluorinated Pd/zirconia was completely inactive toward H₂O₂ synthesis (producing only water), contrary to our results.

To verify whether our Pd-based catalysts were stable and reusable, we carried out some catalytic tests with the ZS–PdO sample already used in a reaction, after filtration and drying. We found that both productivity and selectivity remained unchanged after the third reaction cycle. This result not only demonstrates the excellent reusability of our samples, but also confirms the absence of Pd leaching during kinetic tests.

3.7. Effect of the Pd oxidation state

The effect of Pd oxidation state on catalytic activity has been the matter of some debate in the scientific literature. Choudhary [49,50] claimed that PdO is the best catalyst for the direct synthesis of H₂O₂, whereas other authors, including Lunsford [43], Burch [10], and Thompson [13], reported higher conversions and higher selectivity toward H₂O₂ when Pd was in its reduced state.

Our samples were reddish-brown after calcination; these catalysts are labelled ZX–PdO. During catalytic tests, the color turned from reddish-brown to dark gray or black. TPR experiments confirmed that the Pd reduction occurred during catalysis (see above). These observations are summarized in Fig. 7a. The reduction of the metal particles was clearly linked to the observed change in catalytic behavior shown in Fig. 6; the cat-

alysts became less selective as the reaction proceeded due to a change in the Pd oxidation state.

A catalytic test on reduced ZS–Pd catalyst showed slightly higher productivity with respect to fresh, nonreduced ZS–PdO catalyst, but with more rapidly decreasing selectivity (Fig. 8). These differences could be explained by the β-hydride phase formation observed in Fig. 3b. During Pd reduction, a structural rearrangement may occur (Fig. 7a), leading to the formation of surface defects (more active sites), which could easily account for the improved hydrogenation performance as well as the lower selectivity, as suggested previously [29].

We also tried a preactivation process consisting of particle surface oxidation (Fig. 7b). ZS–PdO catalyst was reduced in situ by passing a pure hydrogen flow into the reaction medium (after the usual deaeration step). This led to a reduced catalyst (with TPR measurements confirming complete reduction of the catalyst). Pure oxygen was fed. Excess oxygen was removed by passing pure nitrogen, after which the nonexplosive H₂/air/N₂ gas mixture was fed into the reactor and H₂O₂ synthesis started. Fig. 8 shows the results and compares them with those of two other tests (with fresh and reduced catalysts). Interestingly, surface oxidation induced very high catalytic activity. In addition, the selectivity was the highest (from 35 to 28%). The maximum H₂O₂ produced was 59 mM (0.2 wt%) with a productivity >800 mmol_{H₂O₂}/(g_{Pd} h). Table 3 provides results of the kinetic analysis of the three catalytic tests. The reduced particles had a higher k'_1 (almost double that of fresh catalyst), but also the highest k'_2 and k'_3 . The reduced and surface-oxidized catalysts showed the highest k'_1 and the lowest k'_2 , at least comparable to that of a fresh catalyst, as was k'_3 . ZF–PdO and ZBr–PdO were similarly preoxidized; Table 3 gives the corresponding kinetic constants. Analysis of Table 3 and Fig. 8 leads to the following observations: (i) surface-oxidized ZS–Pd was the best sample, giving, as stated above, a 0.2 wt% H₂O₂ solution; (ii) both surface-oxidized ZF–Pd and ZBr–Pd showed a significant improvement in catalytic performance with respect to fresh samples; (iii) selectivity always dropped—with different slopes—to low values, indicating that the surface oxide layer is not stable under our reaction conditions; and (iv) the fluorinated sample had the highest k'_1 but also the highest k'_3 .

We attempted to stabilize this surface-oxidized Pd particle state by feeding an undiluted hydrogen/oxygen mixture with

Table 3
Kinetic constants for ZS–PdO pretreated in different conditions and tested under different gas feed

Sample	Gas feed	$k'_1 \times 10^4$ (mol/(l min))	$k'_2 \times 10^4$ (mol/(l min))	$k'_3 \times 10^2$ (min ⁻¹)
ZS–PdO fresh	H ₂ /air/N ₂	5.3	8.7	1.1
ZS–Pd reduced	H ₂ /air/N ₂	9.0	10.4	2.4
ZS–PdO surface oxidized	H ₂ /air/N ₂	9.9	7.9	1.5
ZS–Pd	4%H ₂ /96%O ₂	2.7	3.5	0.051
ZF–PdO fresh	H ₂ /air/N ₂	5.6	7.8	1.3
ZF–PdO surface oxidized	H ₂ /air/N ₂	14.2	8.3	3.5
ZBr–PdO fresh	H ₂ /air/N ₂	3.7	8.9	1.0
ZBr–PdO surface oxidized	H ₂ /air/N ₂	9.2	9.9	1.7

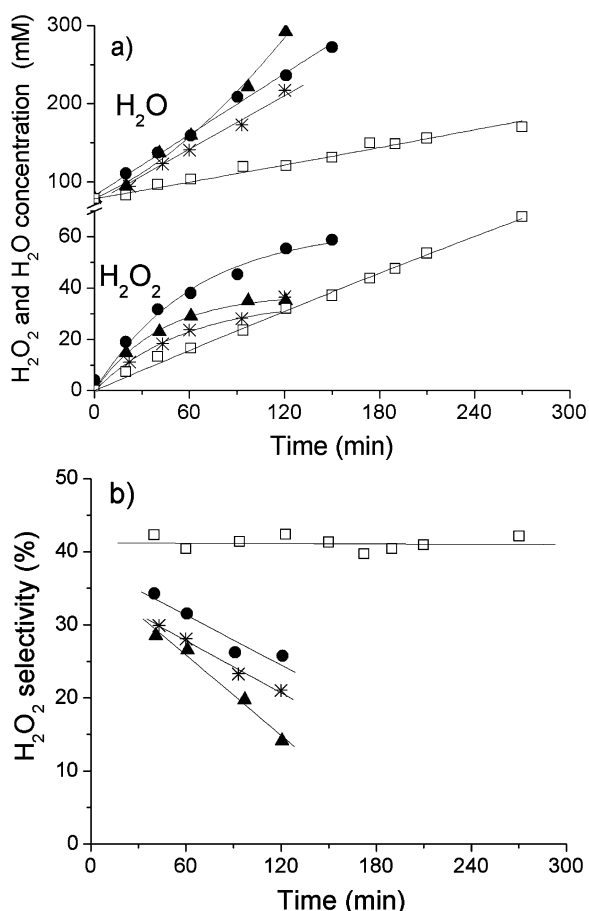


Fig. 8. Activity (a) and selectivity (b) in H₂/air/N₂ of ZS–Pd in its different states Pd (▲), PdO (*), Pd–PdO surface (●), compared to catalytic results of the same sample in 4% H₂ and 96% O₂ gas mixture (□).

oxygen in large excess (H₂:O₂ = 4:96). This is not only outside the explosion range, but also outside the flammable range, and hence is intrinsically safer than the previous experiments. We tested ZS–Pd, our best catalyst, under these new reaction conditions; the results are given in Fig. 8 and Table 3. The catalyst's different behavior in the latter test is noteworthy. The productivity was comparably lower at the beginning, but showed very good values on long reaction times (550 mmolH₂O₂/(gPd h) after 5 h). The most interesting result, however, is the very low water production rate (50 times lower than in air), which corresponds to a significantly higher selectivity toward H₂O₂ (around 40%). Moreover, under these test conditions (large ex-

cess of oxygen, undiluted H₂/O₂ mixture), catalyst selectivity was extremely stable for several hours, meaning that the Pd particle state did not change. It is also noteworthy that under the reaction conditions of Fig. 8, all catalysts showed H₂ conversions (calculated from H₂O₂ + H₂O obtained vs. H₂ fed) in the range of 70–100%.

4. Conclusion

In this work, palladium-based catalysts supported on SO₄²⁻, Cl⁻, F⁻, and Br⁻-doped zirconia were successfully tested for the direct synthesis of hydrogen peroxide under very mild conditions and outside the explosion range. The 2.5% Pd loaded on anion-doped zirconia samples showed good catalytic activity, selectivity, mechanical stability, and reusability. Investigation of the effects of water, ethanol, or methanol as a reaction medium confirmed that best catalytic results could be achieved in methanol, with the attainable H₂O₂ concentrations improved from 3.2–4.4 mM in aqueous solution up to 36 mM under our best experimental conditions.

The importance of surface-oxidized palladium for the reaction can be deduced by TPR analysis and catalytic tests with different gas feeds. High H₂O₂ productivity (550 mmolH₂O₂/(gPd h)) and the highest selectivity (40%, still stable after 5 h) at 72% conversion can be reached under suitable conditions. These results compare with the best findings obtained by Hutchings and coworkers [16] using 5% Pd/TiO₂ but working under pressure (37 bar).

Acknowledgments

The authors acknowledge the financial support of MIUR (Rome). S. Melada and F. Menegazzo thank INSTM (Florence) for postdoctoral fellowships.

References

- [1] H. Henkel, W. Weber, US Patent 110875 (1914).
- [2] Chemical Week, 2003, July 2/9, 44.
- [3] H.-J. Riedl, G. Pfeleiderer, US Patent 2215883 (1940).
- [4] L.W. Gosser, US Patent 4681751 (1987).
- [5] L.W. Gosser, J.T. Schwatrz, US Patent 4772485 (1988).
- [6] J. Van Weynbergh, J.-P. Schoebrechts, US Patent 5447706 (1995).
- [7] B. Bertsch-Frank, I. Hemme, S. Katusic, J. Rollmann, US Patent 6387364 (2002).

- [8] G. Paparatto, R. D'Aloisio, G. De Alberti, R. Buzzoni, US Patent 6630118 (2003).
- [9] T.A. Pospelova, N.I. Kobozev, E.N. Eremin, Russ. J. Phys. Chem. 35 (1961) 143.
- [10] R. Burch, P.R. Ellis, Appl. Catal. B 42 (2003) 203.
- [11] D.P. Dissanayake, J.H. Lunsford, J. Catal. 214 (2003) 113.
- [12] P. Landon, P.J. Collier, A.J. Papworth, C.J. Kiely, G.J. Hutchings, Chem. Commun. (2002) 2058.
- [13] V.V. Krishnan, A.G. Dokoutchaev, M.E. Thompson, J. Catal. 196 (2000) 366.
- [14] A.G. Gaikwad, S.D. Sansare, V.R. Choudhary, J. Mol. Catal. A 181 (2002) 143.
- [15] J.K. Edwards, B. Solsona, P. Landon, A.F. Carley, A. Herzing, M. Watanabe, C. Kiely, G. Hutchings, J. Mater. Chem. 15 (2005) 4595.
- [16] J.K. Edwards, B. Solsona, P. Landon, A.F. Carley, A. Herzing, C. Kiely, G. Hutchings, J. Catal. 236 (2005) 69.
- [17] T.A. Pospelova, N.I. Kobozev, Russ. J. Phys. Chem. 35 (1961) 262.
- [18] L.W. Gosser, J.-A.T. Schwartz, US Patent 4,832,938 (1989).
- [19] L.W. Gosser, M.A. Paoli, US Patent 5,135,731 (1992).
- [20] K. Otsuka, I. Yamanaka, Electrochim. Acta 35 (1990) 319.
- [21] I. Yamanaka, T. Onizawa, S. Takenaka, K. Otsuka, Angew. Chem. Int. Ed. 42 (2003) 3655.
- [22] I. Yamanaka, T. Hashimoto, K. Otsuka, Chem. Lett. (2002) 852.
- [23] Y. Ando, T. Tanaka, Int. J. Hydrogen Energy 29 (2004) 1349.
- [24] M.J. Kirkpatrick, B.R. Locke, Ind. Eng. Chem. Res. 44 (2005) 4243.
- [25] J. Zhou, H. Guo, X. Wang, M. Guo, J. Zhao, L. Chen, W. Gong, Chem. Commun. (2005) 1631.
- [26] J.A. McIntyre, US Patent 5512263 (1996).
- [27] V.R. Choudhary, S.D. Sansare, A.G. Gaikwad, US Patent 6,448,199 (2002).
- [28] V.R. Choudhary, A.G. Gaikwad, S.D. Sansare, Angew. Chem. Int. Ed. 40 (2001) 1776.
- [29] S. Abate, G. Centi, S. Melada, S. Perathoner, F. Pinna, G. Strukul, Catal. Today 104 (2005) 323.
- [30] F. Moseley, P.N. Dyer, US Patent 4,336,240 (1982).
- [31] S.J. Gregg, K.S.W. Sing, Adsorption, Surface Area and Porosity, 2nd ed., Academic Press, 1982, p. 111.
- [32] S. Melada, M. Signoretto, F. Somma, F. Pinna, G. Cerrato, G. Meligrana, C. Morterra, Catal. Lett. 94 (2004) 193.
- [33] M. Signoretto, S. Melada, F. Pinna, S. Polizzi, G. Cerrato, C. Morterra, Microporous Mesoporous Mater. 81 (2005) 19.
- [34] B.H. Davis, R.A. Keogh, R. Srinivasan, Catal. Today 20 (1994) 219.
- [35] R. Srinivasan, R.A. Keogh, D.R. Milburnand, B.H. Davis, J. Catal. 153 (1995) 123.
- [36] S. Ardizzone, C. Bianchi, E. Grassi, Colloids Surf. 135 (1998) 41.
- [37] P.D.L. Mercera, PhD thesis, University of Twente, The Netherlands, (1991) p. 19.
- [38] W. Palczewska, in: Z. Paal, P.G. Menon (Eds.), Hydrogen Effects in Catalysis, Dekker, New York, 1988, p. 373.
- [39] Z. Karpinski, Adv. Catal. 37 (1990) 45.
- [40] G. Paparatto, R. D'Aloisio, G. De Alberti, R. Buzzoni, EP 1160196 A1 (2001).
- [41] T. Haas, G. Stochniol, J. Rollmann, US Patent 6,764,671 B1 (2004).
- [42] Y.-F. Han, J.H. Lunsford, Catal. Lett. 99 (2005) 13.
- [43] S. Chinta, J.H. Lunsford, J. Catal. 225 (2004) 249.
- [44] V.R. Choudhary, C. Samantha, A.G. Gaikwad, Chem. Commun. (2004) 2054.
- [45] P. Paredes Olivera, E.M. Patrito, H. Sellers, Surf. Sci. 313 (1994) 25.
- [46] S. Melada, F. Pinna, G. Strukul, S. Perathoner, G. Centi, J. Catal. 237 (2006) 213.
- [47] V.R. Choudhary, C. Samanta, J. Catal. 238 (2006) 28.
- [48] V.R. Choudhary, A.G. Gaikwad, S.D. Sansare, Catal. Lett. 83 (2002) 235.
- [49] A.G. Gaikwad, S.D. Sansare, V.R. Choudhary, J. Mol. Catal. A 181 (2002) 143.
- [50] V.R. Choudhary, A.G. Gaikwad, S.D. Sansare, US Patent 6,534,440 (2003).